Magnetic-Phase Dependence of the Spin Carrier Mean Free Path in Graphene Nanoribbons

Jing Li,[1,*] Yann-Michel Niquet,[1,†] and Christophe Delerue[2,‡]
[1]Université Grenoble Alpes, INAC-MEM, L_Sim, Grenoble, France and CEA, INAC-MEM, L_Sim, 38000 Grenoble, France
[2]IEMN, UMR CNRS 8520, 59652 Villeneuve d'Ascq, France
(Received 16 December 2015; published 8 June 2016)

We show theoretically that the intrinsic (phonon-limited) carrier mobility in graphene nanoribbons is considerably influenced by the presence of spin-polarized edge states. When the coupling between opposite edges switches from antiferromagnetic to ferromagnetic with increasing carrier density, the current becomes spin polarized and the mean free path rises from 10 nm to micrometers. In the ferromagnetic state, the current flows through one majority-spin channel which is ballistic over micrometers and several minority-spin channels with mean free paths as low as 1 nm. These features predicted in technology-relevant conditions could be nicely exploited in spintronic devices.

DOI: 10.1103/PhysRevLett.116.236602

Graphene nanoribbons (GNRs) [1,2] are very attractive for electronic [3–7] and spintronic [8–14] applications, but the reported carrier mobilities are scattered over four decades [4–6,15–20]. Indeed, the effects of quantum confinement depend not only on the lateral width of a GNR but also on the geometry of its edges, which can be armchair [Fig. 1(a)], zigzag [Fig. 1(b)], or a mixture of both, according to its orientation [1]. Tight-binding (TB) calculations in a single-particle picture predict that armchair GNRs are semiconducting, while zigzag GNRs are metallic but host peculiar flatband edge states [1]. These flat bands, when partially filled, are unstable upon electron-electron interactions. Various models [21–23] thus consistently predict magnetically ordered phases in zigzag GNRs, with spins aligned along the edges (Fig. 1). Depending on the ribbon width and carrier density, the coupling between opposite edges can be antiferromagnetic (AF), which opens a gap in the band structure, or ferromagnetic (F). This behavior has been experimentally observed at room temperature and is well reproduced by TB calculations in which the electron-electron interactions are described by a mean-field Hubbard model [24].

Here, we present calculations demonstrating that the spin-polarized edge states considerably influence the phonon-limited mobility and mean free path (MFP) in zigzag GNRs. At the AF → F transition, the current indeed becomes spin polarized, and the MFP rises from 10 nm to micrometers. In the ferromagnetic state, the current actually flows through very distinct modes: one channel for majority-spin electrons which is ballistic over micrometers, and several channels for minority-spin electrons with MFPs as short as 1 nm. Minority-spin electrons can thus be efficiently filtered out from the current in long enough nanoribbons. Our work also sheds new light on recent experiments on epitaxial GNRs [20], suggesting that the two observed transport channels can be associated with different spins.

We consider GNRs described by the mean-field Hubbard TB model of Ref. [23]:

$$H = \sum_i E_{i,\sigma}\hat{n}_{i,\sigma} + \sum_{i,j,\sigma} t_{i,j}\hat{c}^\dagger_{i,\sigma}\hat{c}_{j,\sigma} + U\sum_i (\hat{n}_{i,\uparrow}\langle n_{i,\downarrow}\rangle + \hat{n}_{i,\downarrow}\langle n_{i,\uparrow}\rangle - \langle n_{i,\uparrow}\rangle\langle n_{i,\downarrow}\rangle), \quad (1)$$

where $\hat{c}^\dagger$ ($\hat{c}$) is a creation (annihilation) operator, and $\hat{n}_{i,\sigma} = \hat{c}^\dagger_{i,\sigma}\hat{c}_{i,\sigma}$ is the number of electrons with spin $\sigma = \uparrow$ or $\downarrow$ on site i. E_i is the on-site energy of the p_z orbital p_i, and $t_{i,j}$ is the nearest-neighbor hopping energy between p_i and p_j, which depend on bond lengths as in Ref. [25]. $U = 3.24$ eV is the Hubbard potential [24]. The band structure

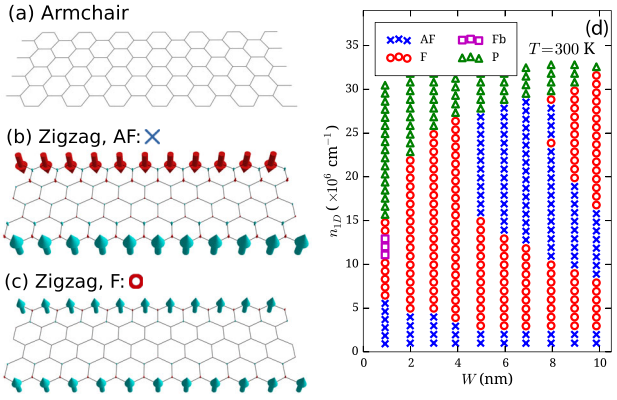

FIG. 1. (a) A 1-nm-wide armchair GNR. (b) Magnetization in a 1-nm-wide zigzag GNR in the antiferromagnetic state ($n_{1D} = 1 \times 10^6$ cm^{-1}, $T = 300$ K). (c) The same in the ferromagnetic state ($n_{1D} = 7 \times 10^6$ cm^{-1}). (d) Magnetic state in zigzag GNRs versus ribbon width W and carrier density n_{1D} ($T = 300$ K).

and spin densities are self-consistently computed from Eq. (1). Among the multiple solutions, which correspond to different magnetic states, we choose the one that minimizes the free energy. By convention, the majority spin in the F state is the spin up (↑).

We then solve exactly the linearized Boltzmann equation for the phonon-limited conductivity σ and mobility μ. The phonons are computed with a fourth-nearest-neighbor force-constant model, and the scattering matrix elements from the derivatives of the TB Hamiltonian with respect to the atomic positions. Details can be found in Ref. [25]. In graphene, the calculated conductivity is in excellent agreement with experiments [26] and *ab initio* data over a wide range of carrier density and temperature [27].

We also compute the ballistic conductance $G_b = -(e^2/h)\int dE T(E)\partial f/\partial E$, where $f(E)$ is the Fermi-Dirac distribution function and $T(E)$ is the ballistic transmission coefficient (see Fig. 3 of the Supplemental Material [28]). The MFP $l_{0\uparrow}$ is then defined as the ribbon length where the phonon-limited conductance $\sigma_\uparrow/l_{0\uparrow}$ of spin-up electrons is equal to the ballistic conductance $G_{b\uparrow}$ (and the same for spin down). In order to interpret these composite values, we also define the MFP in each band, $l^m_{p,k,\sigma} = 2|v_{p,k,\sigma}|\tau_{p,k,\sigma}$, where $v_{p,k,\sigma}$ is the group velocity, $\tau_{p,k,\sigma}$ the relaxation time, k the wave vector, and p the band index.

The magnetic state of a zigzag GNR depends on the GNR width W, the carrier density per unit length n_{1D} (or equivalently the areal density $n_{2D} = n_{1D}/W$), and the temperature T [Fig. 1(d)] [23]. At $T = 300$ K, the magnetic state of a narrow ribbon ($2 \le W \le 4$ nm) follows the sequence AF → F → paramagnetic (P) when n_{1D} increases. There is an extra oscillation between the AF and F states in wider GNRs, and an additional ferromagnetic state with broken symmetry (Fb) in the narrowest ones. Similar phase diagrams are obtained at $T = 0$ K and $T = 77$ K (Fig. 1 in the Supplemental Material [28]). At lower temperatures, the Fb phase is more ubiquitous, and the first transition from AF to F, as well as the transition to the P state, occur at lower carrier densities than at $T = 300$ K.

Figure 2 shows typical band structures near the Fermi level of the AF and F states. Band structures on a larger scale are plotted in Fig. 2 of the Supplemental Material [28]. A band gap only exists in the AF state and vanishes at the AF → F transition. In agreement with the experiments of Ref. [24], we recover this transition at about $W = 7.5$ nm for $n_{2D} = 2.9 \times 10^{12}$ cm^{-2} [Fig. 3(a)]. Our calculations demonstrate that the magnetic state has a huge impact on the transport properties. When W increases, the phonon-limited carrier mobility raises abruptly by 2 orders of magnitude (10^3 to 10^5 cm^2/V/s) at the AF → F transition [Fig. 3(b)]. Before the transition, the mobility is proportional to $W^{3.2}$. Interestingly, such a power law dependence has already been found in semiconducting

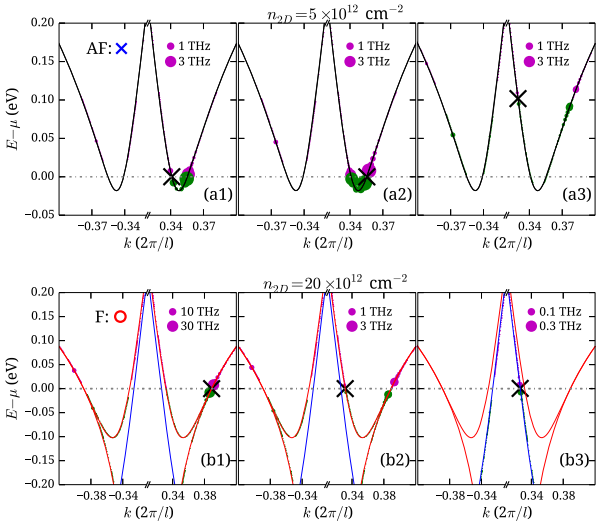

FIG. 2. Room-temperature band structures and scattering rates in a 5-nm-wide zigzag GNR. (a1)–(a3) Close-up near the Fermi level μ in the AF state ($n_{2D} = 5 \times 10^{12}$ cm^{-2}). The scattering rates from a given initial state, marked with a cross, are plotted on top of the band structure. They are proportional to the diameter of the dots (see the scale in each panel). The green (pink) dots label the possible final states after phonon emission (absorption). (b1)–(b3) The same in the F state ($n_{2D} = 20 \times 10^{12}$ cm^{-2}). Spin-up (-down) bands are shown in blue (red). Relevant spin distributions and wave functions are shown in Figs. 4 and 5 of the Supplemental Material [28].

zigzag carbon nanotubes [25,29], but here the gap is induced by the magnetic coupling between the edges. At the AF → F transition, the mobility jumps near the value in graphene [25]. Similar trends are found for a larger density $n_{2D} = 20 \times 10^{12}$ cm^{-2} (Fig. 6 in the Supplemental Material [28]).

Similarly, the AF → F transition can be induced by increasing n_{2D}. This also enhances the carrier mobility tremendously [Fig. 4(a)]. In a 5-nm-wide zigzag GNR, μ increases by about 2 orders of magnitude at the AF → F transition around $n_{2D} = 6 \times 10^{12}$ cm^{-2} ($T = 300$ K). The oscillation between the AF and F states at larger carrier densities also has a huge impact on the mobility, e.g., at the F → AF transition near $n_{2D} = 32 \times 10^{12}$ cm^{-2}. The variations of the mobility are nonetheless smaller at large n_{2D}'s because the Fermi level is far above the bottom of the edge state bands (see Fig. 7 in the Supplemental Material [28]). When the edge state bands are completely filled, the GNR goes into the P state. The mobility then peaks when the Fermi level lies between the edge states and the next conduction bands (near $n_{2D} = 60 \times 10^{12}$ cm^{-2} in a 5-nm-wide zigzag GNR). These huge variations of the mobility are highlighted here at $T = 300$ K, for technology-relevant carrier densities, in situations where the changes of the ballistic conductances [Fig. 4(b)] are much smaller, even if they are not negligible [9,11].

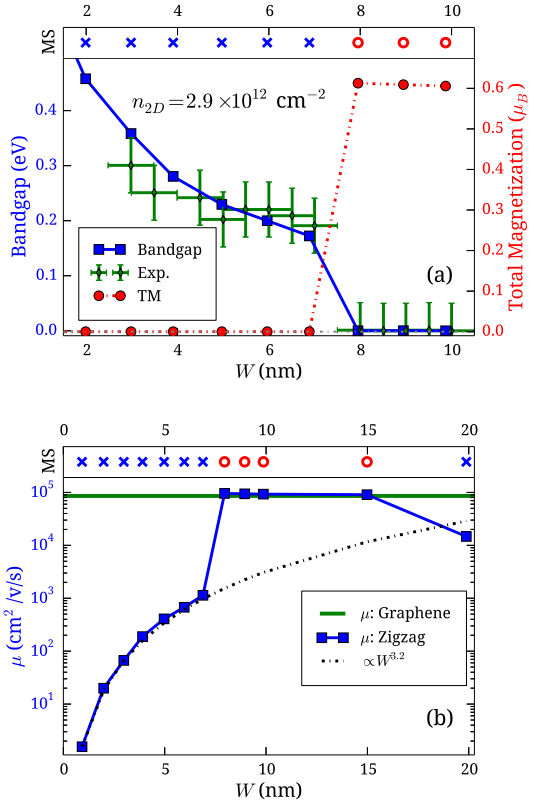

FIG. 3. Mobility and magnetoelectronic state versus ribbon width in zigzag GNRs ($n_{2D} = 2.9 \times 10^{12}$ cm^{-2}, $T = 300$ K). (a) Band gap (blue squares) and total magnetization per unit cell (red dots). Experimental data (green error bars) are from Ref. [24]. (b) Carrier mobility. The green solid line is the mobility in graphene. The magnetic state (MS) is indicated using the same symbols as in Fig. 1.

These results suggest that the MFP of the carriers depends considerably on the magnetic state. For a 5-nm-wide zigzag GNR in the AF state [$n_{2D} < 3 \times 10^{12}$ cm^{-2}, Fig. 4(b)], the MFP is about 15 nm ($l_{0\uparrow} = l_{0\downarrow}$), in agreement with the experiments of Ref. [5]. The MFP for spin-up electrons, $l_{0\uparrow}$, jumps from 15 nm to 4–7 μm at the AF $\rightarrow$ F transition, while $l_{0\downarrow}$ remains around 10 nm.

To get a better understanding of the underlying physics, we plot selected scattering rates in Fig. 2, and the MFP l^m in each channel of the F state in Fig. 4(d). In the AF state, the group velocity v is vanishingly small near the conduction band minimum. The backscattering by long wavelength acoustic phonons is enhanced by the large ($\propto 1/|v|$) density of final states with positive and negative group velocities, so that both v and τ become limited in the MFP $l \equiv |v|\tau$. In the F state, the two spin-down bands that are almost degenerate at large $|k|$ are localized edge states [Fig. 2(b1), and Fig. 5 of the Supplemental Material [28]]. This considerably strengthens the interactions with the family of "breathinglike" phonon modes whose amplitude is maximal but opposite at the two edges. These two channels are, therefore, characterized by very small MFPs (of the order of 1 nm). Although the third spin-down channel is far less localized and more dispersive (larger v), the carriers get rapidly scattered to the former two edge channels by the breathing modes [Fig. 2(b2)], which limits the MFP to ~100 nm. The value of $l_{0\downarrow}$ discussed above is, therefore, an average over three channels with very distinct MFPs. The electrons in the very dispersive spin-up channel remain weakly coupled to phonons because there is no other channel to scatter to for majority spins, and because $k \rightarrow -k$ backscattering, which is dominated by the confined K phonons of graphene, is unlikely. We conclude that the transport in the F state is ballistic for the majority spin and diffusive for the minority spin in a wide range of GNR lengths $L \approx 100$–1000 nm.

The magnetic-phase transitions are therefore accompanied by sudden variations of the spin currents [Fig. 4(c)]. In the AF state, the conductivities $\sigma_\uparrow$ and $\sigma_\downarrow$ are equal because the two opposite edges of the GNR carry the same current but with opposite spins. In the F state, the diffusive spin filtering factor, defined as $(\sigma_\uparrow - \sigma_\downarrow)/(\sigma_\uparrow + \sigma_\downarrow)$, is positive and reaches ≃99%. The transport in the diffusive regime is, therefore, dominated by (majority) spin-up electrons. On the contrary, the ballistic spin filtering factor, defined as $(G_{b\uparrow} - G_{b\downarrow})/(G_{b\uparrow} + G_{b\downarrow})$, is negative because there are three spin-down channels [$G_{b\downarrow} \approx 3e^2/h$, Figs. 4(c) and 4(d)], but only one spin-up channel ($G_{b\uparrow} = e^2/h$). In other words, the spin-down electron current prevails in short GNR devices but vanishes in long enough ones.

Similar behaviors are predicted in chiral GNRs with chiral angles between 0° (zigzag) and 19.1° (Figs. 9 and 10 in the Supplemental Material [28]). Huge variations of the carrier mobility come again with magnetic state transitions.

So far, the experiments on lithographically patterned GNRs report mobilities ranging from 100 to 3500 cm^2/V/s [4–6,15–19] for $n_{2D} \simeq 10^{12}$ cm^{-2}, much lower than in graphene (10^5 cm^2/V/s) [2,30,31]. Of course, these low mobilities may be due to, e.g., defects or disorder at the GNR edges. However, our results show that an intrinsic factor, the magnetic state of the GNR, also plays an important role. In a 10-nm-wide zigzag GNR, the mobility at $n_{2D} \sim 2.5 \times 10^{12}$ cm^{-2} varies by a factor of 30 at the AF $\rightarrow$ F transition (Fig. 7 in the Supplemental Material [28]). If the GNR edges are strongly disordered, fluctuations of the magnetic state along the ribbon might, however, scatter the carriers.

In contrast to lithographically patterned GNRs, excellent transport properties have been reported in 40-nm-wide epitaxial GNRs with nearly zigzag edges [20]. The measured conductance is $G \simeq 2G_0$ in short GNRs with lengths $0.1 < L \lesssim 0.16$ μm, and $G \simeq G_0$ in long GNRs with lengths $1 \lesssim L \lesssim 16$ μm. Our calculations, pushed at their limits, show that a 40-nm-wide GNR is stabilized in the F state at realistic carrier densities (see the Supplemental Material [28]). Our results support many important conclusions of Ref. [20]—in particular, that the transport is

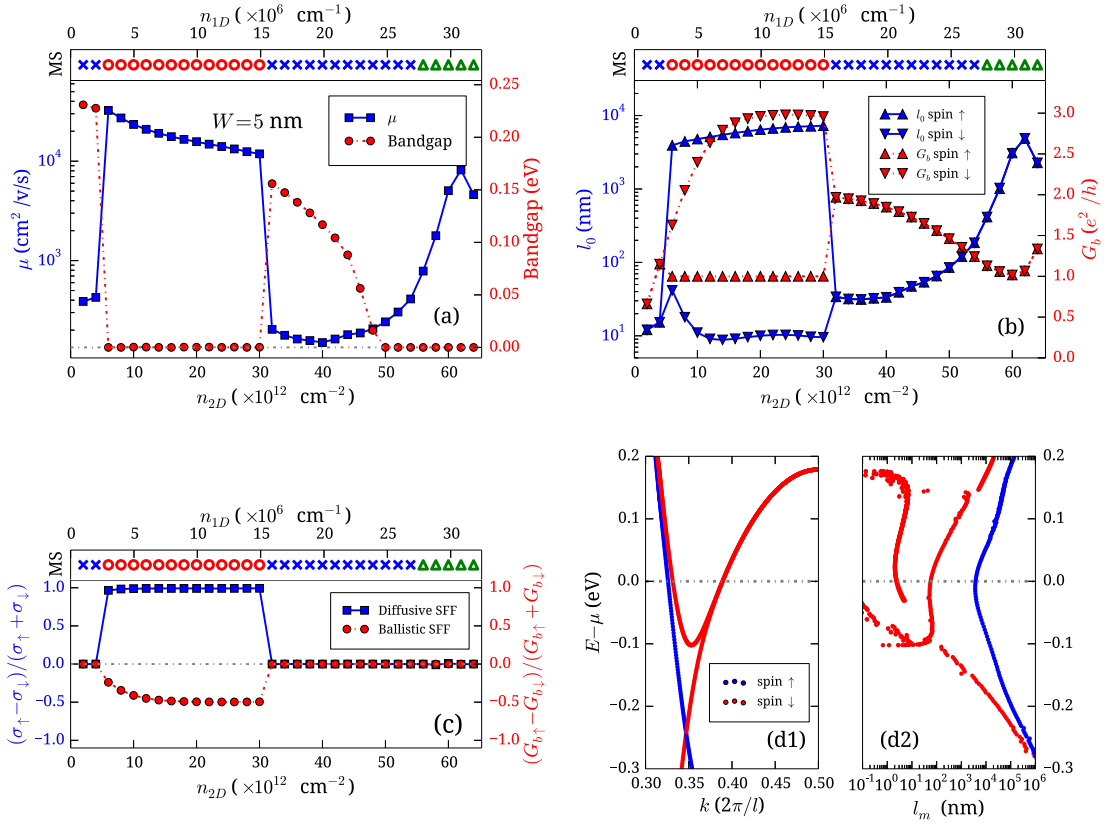

FIG. 4. Mobility, conductance, spin polarization, and MFP in zigzag GNRs ($W = 5$ nm, $T = 300$ K). (a) Carrier mobility (blue squares) and band gap (red dots) versus n_{2D}. (b) MFP l_0 (blue) and ballistic conductance G_b (red) versus n_{2D}, for each spin. (c) Ballistic $[(G_{b\uparrow} - G_{b\downarrow})/(G_{b\uparrow} + G_{b\downarrow})]$ (red dots) and diffusive $[(\sigma_\uparrow - \sigma_\downarrow)/(\sigma_\uparrow + \sigma_\downarrow)]$ (blue squares) spin filtering factor versus n_{2D}. (d) Band structure and MFP l_m in each band as a function of energy, at $n_{2D} = 20 \times 10^{12}$ cm^{-2}. The magnetic state (MS) is indicated using the same symbols as in Fig. 1.

dominated by two channels with very distinct behaviors. Since the experimental GNRs are longer than 100 nm, the two spin-down channels with the shortest MFPs shall indeed be completely turned off. The experimental transport length scales, $L_1 = 160$ nm and $L_2 = 16$ μm, are comparable to the MFPs calculated in the 40-nm-wide GNR for the remaining minority- and majority-spin channel (Fig. 8 in the Supplemental Material [28]). The measured conductance (G), however, decays exponentially between the $G = 2G_0$, $G = G_0$, and $G = 0$ plateaus, which is the fingerprint of a nondiffusive transport regime. We emphasize that the coupling to phonons is so weak in these two channels that the transport might indeed become nondiffusive in the presence of additional elastic scattering. However, the ratio between the MFPs shall remain representative of the characteristic length scales in these two channels. Whatever the disorder, the majority-spin electrons in particular cannot scatter to the edge states due to spin blocking, in contrast to minority-spin electrons. We therefore suggest that the current is not spin polarized on the $2G_0$ plateau measured in short GNRs (two channels with opposite spins), while the minority spin-down electrons are filtered out on the G_0 plateau measured in long GNRs. These efficient spin-filtering properties could be nicely exploited in spintronic devices.

In summary, our results demonstrate that a GNR field-effect transistor can switch from an on state in a ballistic regime (high carrier density, F state, spin-polarized current) to an intermediate state in a diffusive regime (lower carrier density, low mobility, AF state), and then to an off state in a depleted regime allowed by the presence of a gap in the AF state. In the F state, the system can be described by a three-current model in which the channel for majority-spin carriers has a MFP in the micrometer range, and the channels for minority-spin carriers have MFPs in the 1 to 100 nm range. This unusual behavior, combined with the small spin-orbit coupling of carbon [2], confirms that GNRs are very promising for spintronic applications [8–14].

J. L. gratefully acknowledges the helpful discussion with Léo Bourdet and Ivan Duchemin. This work was supported by French National Research Agency (ANR) Project No. "NOODLES" ANR-13-NANO-0009-02. Part of the calculations were run on the TGCC/Curie machine, using allocations from GENCI and PRACE.

*jing.li.phy@gmail.com
†yniquet@cea.fr
‡christophe.delerue@isen.fr

[1] K. Nakada, M. Fujita, G. Dresselhaus, and M. S. Dresselhaus, Phys. Rev. B **54**, 17954 (1996).
[2] A. H. Castro Neto, F. Guinea, N. M. R. Peres, K. S. Novoselov, and A. K. Geim, Rev. Mod. Phys. **81**, 109 (2009).
[3] Q. Yan, B. Huang, J. Yu, F. Zheng, J. Zang, J. Wu, B.-L. Gu, F. Liu, and W. Duan, Nano Lett. **7**, 1469 (2007).
[4] Z. Chen, Y.-M. Lin, M. J. Rooks, and P. Avouris, Physica E (Amsterdam) **40E**, 228 (2007).
[5] X. Wang, Y. Ouyang, X. Li, H. Wang, J. Guo, and H. Dai, Phys. Rev. Lett. **100**, 206803 (2008).
[6] M. Y. Han, J. C. Brant, and P. Kim, Phys. Rev. Lett. **104**, 056801 (2010).
[7] W. S. Hwang, P. Zhao, K. Tahy, L. O. Nyakiti, V. D. Wheeler, R. L. Myers-Ward, C. R. Eddy, D. K. Gaskill, J. A. Robinson, W. Haensch, H. G. Xing, A. Seabaugh, and D. Jena, APL Mater. **3**, 011101 (2015).
[8] Y.-W. Son, M. L. Cohen, and S. G. Louie, Nature (London) **444**, 347 (2006).
[9] W. Y. Kim and K. S. Kim, Nat. Nanotechnol. **3**, 408 (2008).
[10] O. V. Yazyev and M. I. Katsnelson, Phys. Rev. Lett. **100**, 047209 (2008).
[11] F. Muñoz-Rojas, J. Fernández-Rossier, and J. J. Palacios, Phys. Rev. Lett. **102**, 136810 (2009).
[12] J. Bai, R. Cheng, F. Xiu, L. Liao, M. Wang, A. Shailos, K. L. Wang, Y. Huang, and X. Duan, Nat. Nanotechnol. **5**, 655 (2010).
[13] B. Dlubak, M.-B. Martin, C. Deranlot, B. Servet, S. Xavier, R. Mattana, M. Sprinkle, C. Berger, W. A. De Heer, F. Petroff, A. Anane, P. Seneor, and A. Fert, Nat. Phys. **8**, 557 (2012).
[14] H. Zhang, Z. Ma, and J.-F. Liu, Sci. Rep. **4**, 6464 (2014).
[15] K. Todd, H.-T. Chou, S. Amasha, and D. Goldhaber-Gordon, Nano Lett. **9**, 416 (2009).
[16] L. Jiao, X. Wang, G. Diankov, H. Wang, and H. Dai, Nat. Nanotechnol. **5**, 321 (2010).
[17] Y.-S. Shin, J. Y. Son, M.-H. Jo, Y.-H. Shin, and H. M. Jang, J. Am. Chem. Soc. **133**, 5623 (2011).
[18] M.-W. Lin, C. Ling, L. A. Agapito, N. Kioussis, Y. Zhang, M. M.-C. Cheng, W. L. Wang, E. Kaxiras, and Z. Zhou, Phys. Rev. B **84**, 125411 (2011).
[19] X. Wang, Y. Ouyang, L. Jiao, H. Wang, L. Xie, J. Wu, J. Guo, and H. Dai, Nat. Nanotechnol. **6**, 563 (2011).
[20] J. Baringhaus, M. Ruan, F. Edler, A. Tejeda, M. Sicot, A. Taleb-Ibrahimi, A.-P. Li, Z. Jiang, E. H. Conrad, C. Berger, C. Tegenkamp, and W. A. de Heer, Nature (London) **506**, 349 (2014).
[21] Y.-W. Son, M. L. Cohen, and S. G. Louie, Phys. Rev. Lett. **97**, 216803 (2006).
[22] L. Yang, M. L. Cohen, and S. G. Louie, Phys. Rev. Lett. **101**, 186401 (2008).
[23] J. Jung and A. H. MacDonald, Phys. Rev. B **79**, 235433 (2009).
[24] G. Z. Magda, X. Jin, I. Hagymási, P. Vancsó, Z. Osváth, P. Nemes-Incze, C. Hwang, L. P. Biró, and L. Tapasztó, Nature (London) **514**, 608 (2014).
[25] J. Li, H. Pereira Coutada Miranda, Y.-M. Niquet, L. Genovese, I. Duchemin, L. Wirtz, and C. Delerue, Phys. Rev. B **92**, 075414 (2015).
[26] D. K. Efetov and P. Kim, Phys. Rev. Lett. **105**, 256805 (2010).
[27] C.-H. Park, N. Bonini, T. Sohier, G. Samsonidze, B. Kozinsky, M. Calandra, F. Mauri, and N. Marzari, Nano Lett. **14**, 1113 (2014).
[28] See Supplemental Material at http://link.aps.org/supplemental/10.1103/PhysRevLett.116.236602 for the phase diagrams at 77 and 300 K, and for additional results for zigzag GNRs and armchair or chiral GNRs.
[29] V. Perebeinos, J. Tersoff, and P. Avouris, Phys. Rev. Lett. **94**, 086802 (2005).
[30] S. V. Morozov, K. S. Novoselov, M. I. Katsnelson, F. Schedin, D. C. Elias, J. A. Jaszczak, and A. K. Geim, Phys. Rev. Lett. **100**, 016602 (2008).
[31] K. I. Bolotin, K. J. Sikes, J. Hone, H. L. Stormer, and P. Kim, Phys. Rev. Lett. **101**, 096802 (2008).